Design Optimization and Characterization of a 3-D-Printed Tactile Sensor for Tissue Palpation

D. Lo Presti, *Member, IEEE*, L. Zoboli, A. Addabbo, D. Bianchi, A. Dimo, *Student Member, IEEE*, C. Massaroni, *Senior Member, IEEE*, V. Altomare, A. Grasso, A. Gizzi, *Senior Member, IEEE*, and E. Schena, *Senior Member, IEEE*

***Abstract*—Manual palpation is a crucial medical procedure that relies on surface examination to detect internal tissue abnormalities, heavily reliant on healthcare professionals' expertise and tactile sensitivity. To tackle these issues, smart palpation systems based on electrical or optical sensors have been developed to perform quantitative tactile measurements, crucial for identifying various solid tumors, including breast and prostate cancer by assessing tissue mechanical properties. In this context, fiber Bragg gratings (FBGs) are emerging as a an ideal candidate for tactile sensing due to their advantages (e.g., high metrological properties, multiplexing capacity, and easy packaging). This study explores the benefits of FBG and 3-D printing to develop a tactile sensor for tissue palpation. First, an optimization of the design of the sensing core of a previously developed probe was conducted through finite element analysis. The novel structure addresses the primary limitation of the previous solution, where nonuniform strain distribution on the encapsulated FBG causes compression on the grating with high risk of bending and breakage. In contrast, the modeled geometry ensures FBG elongation during tissue palpation. A 3-D printing and characterization of the proposed solution was carried out to investigate the response of the enclosed FBG when pushed against different materials showing promising results in discriminating tissues according to their mechanical properties: the more rigid the indented substrate, the higher the sensor output. This property will be fundamental for enhancing early tumor detection through superficial tissue palpation, advancing the efficacy of prevention measures.**

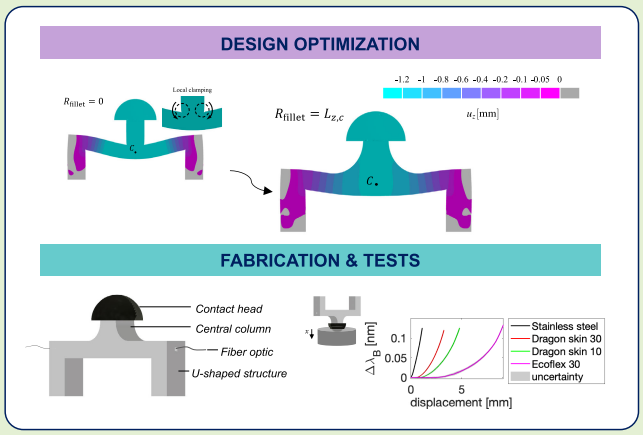

***Index Terms*— 3-D printing, additive manufacturing, fiber Bragg gratings (FBGs), tactile sensing, tissue palpation.**

Manuscript received 12 January 2024; revised 16 February 2024; accepted 16 February 2024. Date of publication 29 February 2024; date of current version 16 April 2024. The work of L. Zoboli, D. Bianchi, and A. Gizzi was supported by the Italian National Group for Mathematical Physics (GNFM-INdAM). The work of D. Bianchi was supported by the Italian Ministry of University and Research (MIUR) through Programma Operativo Nazionale (PON) "Ricerca e Innovazione" 2014–2020 (azione IV.6)-FSE-REACT EU. The associate editor coordinating the review of this article and approving it for publication was Dr. A Theodosiou. *(Corresponding author: D. Lo Presti.)*

D. Lo Presti, A. Addabbo, A. Dimo, C. Massaroni, and E. Schena are with the Unit of Measurements and Biomedical Instrumentation, Department of Engineering, Università Campus Bio-Medico di Roma, 00128 Rome, Italy, and also with the Fondazione Policlinico Universitario Campus Bio-Medico, 00128 Rome, Italy (e-mail: d.lopresti@unicampus.it).

L. Zoboli, D. Bianchi, and A. Gizzi are with the Unit of Nonlinear Physics and Mathematical Modeling, Department of Engineering, Università Campus Bio-Medico di Roma, 00128 Rome, Italy (e-mail: l.zoboli@unicampus.it; d.bianchi@unicampus.it; a.gizzi@unicampus.it).

V. Altomare and A. Grasso are with the Breast Surgery Unit, Fondazione Policlinico Universitario Campus Bio-Medico, 00128 Rome, Italy (e-mail: v.altomare@policlinicocampus.it; a.grasso@policlinicocampus.it).

Digital Object Identifier 10.1109/JSEN.2024.3369337

I. Introduction

THE manual palpation of soft tissues is a complex medical procedure, wherein healthcare professionals superficially examine the human body to detect abnormalities within the inner tissue structures [1], [2]. Although it has been widely used for the initial identification and screening of pathological conditions, practitioners rely on their experience and the sensing capacities of their hands or fingers to explore soft body abnormalities (e.g., cancers, abdominal aortic aneurysms, and others) [1], [3]. This approach makes tissue palpation subjective and qualitative. To overcome this issue, a range of techniques based on a variety of sensing technologies have been proposed for performing a quantitative analysis of tissue mechanical properties during palpation [4], [5], [6]. Their working principle relies on pushing a sensorized probe against the tissue surface to measure its mechanical response. A change in the mechanical properties of soft tissues is a useful marker for identifying cancers and has been used in clinical palpation diagnosis for a wide variety of solid tumors,

including breast and prostate cancer [7], [8]. Both these cancers may not initially cause symptoms. Hence, their early-stage identification using unobtrusive techniques symptoms can give the best chance to improve patient safety and surgery outcomes. To date, techniques for tactile sensing mainly rely on piezoresistive, capacitive, and polyvinylidene fluoride (PVDF) sensors [9], [10]. Nevertheless, these systems still face certain limitations, including stringent manufacturing procedures, intricate packaging processes, fragility, limited sensitivity to quasi-static forces, and reduced reliability [9], [10]. Other noninvasive tools for evaluating the stiffness of a lesion are ultrasound elastography [11], [12] or magnetic resonance elastography [13], [14]. Although those are powerful techniques, they also have certain limitations, such as low spatial resolution, operator dependency, and high costs. A technology that can overcome the issue of low resolution is the atomic force microscopy (AFM). Indeed, AFM is a powerful tool to characterize surfaces at nanoscale, but it is technically challenging with problems in obtaining high-quality images at high imaging speed [15], [16].

Most of these issues can be solved by using fiber optic sensors (FOSs) owing to their numerous advantages, such as small size, high frequency response, and high sensitivity [17], [18]. In addition, compared to other sensing technologies, FOSs offer high flexibility and biocompatibility and are resistant to electromagnetic interferences and electrically passive. These features make them outstanding candidates for tactile measurements. The most used FOSs applied to tissue palpation are fiber Bragg gratings (FBGs) [19], [20], [21]. Their use in this scenario can be motivated by the FBGs easy integration into different packaging solutions (e.g., flexible silicones and 3-D printing materials) and multiplexing along a single optical fiber to sense exerted forces with high spatial resolution [22], [23], [24], [25], [26]. FBGs working principle relies on the wavelength demodulation principle, which is not affected by light intensity changes caused by either light power or transmission path [27]. Moreover, FBGs usually work in reflection. This method requires the sensor connection to an interrogation unit from a single side of the optical fiber, supporting easy manufacturing processes, packaging solutions, and system utilization in real scenarios. However, most of the proposed FBG-based tactile probes are realized by directly pasting the optical fiber on the structure body, reducing the reproducibility of the manufacturing process and the repeatability of the sensor response to mechanical inputs [19], [28], [29], [30], [31]. In fact, the glue layer between the sensor and the probe may dampen the measurement transmission from the probe-tissue contact area to the enclosed FBG.

A potential solution to these challenges is represented by the combined use of FBG and 3-D printing techniques, whose advantages allow easy structural design customization of the tactile probes with controllable geometry, miniaturized size, and lightness [25]. To date, only a few 3-D-printed sensors based on FBG technology have been used in clinical applications, including tissue palpation, but most still glue the optical fiber to the printed structures to guarantee a secure optical fiber alignment during its embedment [19], [28], [29], [30], [31]. To the best of our knowledge, we were the first to develop a tactile probe for soft tissue (i.e., breast) palpation that combines FBG in 3-D-printing technology without using glue at the interface between the optical fiber and the printed layer [32]. The structural design of this previous attempt is a U-shaped beam with a vertical body named "central column" and a semispherical contact head placed above for indenting the soft tissue and localizing the mechanical response in the central part of the beam where the FBG is located. However, although the FBG sensor was aligned within the central part of the web in order to undergo tension under the application of force (F) inputs on its contact head, the central column caused a clamping effect on the enclosed FBG, resulting in a grating compression with potential damages during operation.

The present study aims at proposing an optimization of the design of the sensing core of the tactile probe developed in [32] guided by a finite element model (FEM) to allow the proposed structure to experience 1-D strain distribution with higher positive values, where the FBG is located. This causes sensor elongation under external F with a reduction in the risk of breakage. Once the optimal design had been carefully modeled, the sensor was fabricated by the fused deposition modeling (FDM) technique, and its response was characterized on materials with a different rigidity to better investigate the changes in the tactile sensor response according to Young's modulus (E) of the indented substrates. This property will enhance the early tumor detection capabilities of the developed tactile probe since tissues showed increased rigidity during tumorigenesis.

II. Sensing Principle and Structural Design

A. Sensing Principle

An FBG sensor consists of a portion of the optical fiber, in which the refractive index of its core is periodically modulated to form a grating structure [27]. When the light travels through the fiber and hits the grating, an extremely narrow reflection band occurs. This key feature is described by the Bragg condition

$$\lambda_B = 2\, n_{\text{eff}} \Lambda \tag{1}$$

where λ_B is the specific wavelength value at which the reflected spectrum is centered, n_{eff} is the effective refractive index of the fiber core, and Λ is the grating period. The changes in temperature (ΔT) and strain (ε) can alter both n_{eff} and Λ, causing a shift of λ_B ($\Delta\lambda_B$) as

$$\Delta\lambda_B = \lambda_B(1 - p_e)\varepsilon + \lambda_B(\alpha + \xi)\Delta T \tag{2}$$

with p_e, the effective photoelastic coefficient of the silica, α, the thermal expansion coefficient, and ξ, the thermo-optic coefficient [27].

FBGs are well-suited for tension sensing due to their linear response ε. In contrast, in the case of compression, gratings can be easily bent with a high risk of damage or breakage during operation [see (2)].

Hence, this study proposed the optimization of the structural design of the FBG-based sensing core of the tactile probe in [32] to undergo tension under F. It means that the enclosed FBG is expected to experience a positive $\Delta\lambda_B$ with F [33], [34]. Fig. 1 helps to better understand the working principle of the FBG inside the proposed structural design. When pushed against a soft tissue and reaches a harder material (e.g., a tumor), a flexion of the structure occurs with

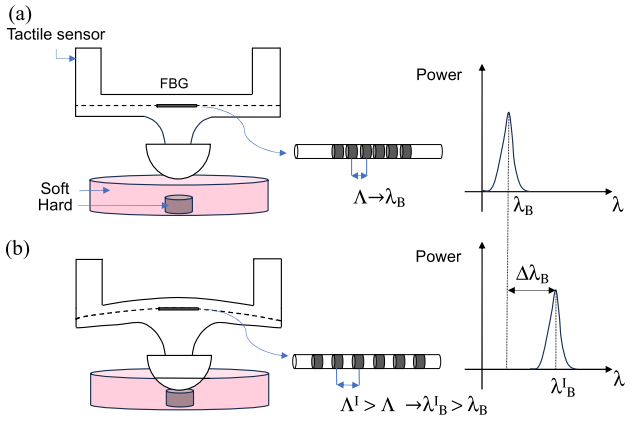

Fig. 1. Working principle of the FBG sensor enclosed in the designed structure in the scenario of interest (i.e., tissue palpation). (a) Output of the sensor when pushed on the surface of soft tissue (e.g., breast). (b) Output of the sensor when encounters harder tissue (e.g., tumor).

TABLE I
GEOMETRY DIMENSIONS

Symbol	Quantity	Value [mm]
$L_{x,s}$	Free span of the sensor	23.54
$L_{x,f}$	Length of the lateral columns	4.28
L_y	Thickness of the device	5.00
L_z	Height of the lateral columns	10.55
$L_{z,f}$	Along-z insertion in base	3.00
$L_{z,c}$	Height of the central column	5.95
R_{sph}	Head radius	5.00

a consequent FBG elongation. This causes an increment of the FBG output from λ_B to λ_B^I (see Fig. 1). As regards the T influence, it can be considered negligible. Indeed, during superficial tissue palpation, the proposed sensor will contact the body using the semispherical head printed in acid polylactic (PLA). Hence, the FBG will not be directly exposed to T change and any effect due to thermal expansion coefficient of the encapsulation 3-D-printed materials is expected to do not cause any considerable changes on the sensor output.

B. Structural Design Optimization via FEM Analysis

The structural design optimization of the sensor core in [32] was guided by a FEM analysis. To better describe the model, we introduce the coordinate system $\{O, x, y, z\}$, positioned at the lowermost plane on the vertical symmetry axis (the z-axis), as shown in Fig. 1, while the associated dimensions are given in Table I. A force, $F_z < 0$ (i.e., downward), is applied on the hemispherical head of the device to simulate compression exerted on the sensor. Null displacements ($u_x = u_y = u_z = 0$) are prescribed to the lower external faces of the lateral columns, $A_{x,f}$, $A_{y,f}$, and $A_{z,f}$, to represent the insertion of the device into an external support that allows the positioning of the sensor onto the tissue (Fig. 2). For the material properties, the body of the device is made of thermoplastic polyurethan—TPU95A ($E = 26$ MPa and $\nu = 0.49$), whereas the head is made of PLA ($E = 0.26$ MPa and $\nu = 0.3$). The geometry has been discretized with displacement-based quadratic hexahedra, creating a structured mesh wherever possible. The total number of nodes is about $107 \cdot 10^3$, and the number of degrees of freedom solved is $310 \cdot 10^3$.

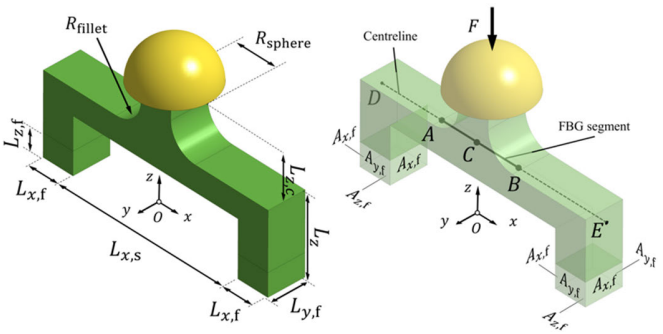

Fig. 2. Geometry (left) and boundary conditions (right) of the analyzed sensor.

To optimize the response of the sensor in [32], we proposed a change in the value of the fillet radius (R_{fillet}) of the central column [32]. In fact, the results in [32] underlined how the absence of a fillet ($R_{\text{fillet}} = 0$) induced a nonnegligible effect of the central column sustaining the contact head of the tactile probe consisting in a local clamping action on the horizontal span of the U-shape under F_z (see Fig. 2). This effect led to a reduction of $\Delta\lambda_B$ with F_z; hence, the FBG was forced to undergo in compression instead of tension with potential fiber optic bending effects and breakages.

The design optimization in the present study was carried out by investigating the behavior of the sensing core of the tactile probe in [32] by varying R_{fillet}, which connects the central column (of height $L_{z,c}$) to the main structure, in the interval $R_{\text{fillet}} = [0, L_{z,c}]$ in steps of 0.5 mm and the intensity of the applied force $F_z = [1, 9]$ N in steps of 2 N.

The structural response of the FBG segment was studied in terms of the average axial strain $\langle \varepsilon_x \rangle$, where the average on a line segment of a function $f(x)$ is defined as $\langle f \rangle = \int_A^B f(x)\mathrm{d}x / \|AB\|$, A and B being the starting and ending points of a segment AB directed along the x-direction, and $\|AB\|$ representing its length. In our FEM analysis, we have assumed perfectly bonded contacts between the FBG and the surrounding structure. Therefore, it was possible to study the effects on the FBG without modeling it as a separate body. Indeed, if the position of the segment AB is chosen to be coincident with the FBG, the computed $\langle \varepsilon_x \rangle$ gives an indication of the average ε_x experienced by the sensor.

To optimize the proposed geometry, we analyzed the effects of a variation of R_{fillet} and F_z separately, focusing on the response along the FBG segment (AB). The effects of the increase of R_{fillet} at a fixed vertical force F_z are shown in Figs. 2–4 (left). Considering the midpoint C of the centerline AB, from Fig. 3, it can be observed that the intensity of the vertical displacement u_z of the midpoint decreases with R_{fillet}, which means that a larger fillet increases the structure stiffness along the vertical direction. This is an expected result because the presence of a fillet allows the distribution of the load F_z along a wider length of the centerline when compared to the no-fillet case.

It is worth recalling, from basic beam theory, that the deflection of a supported beam is higher when there is a concentrated load at its midpoint and smaller when the same load is distributed along the whole centerline. On the other hand, the behavior along the axial direction x results from the combination of a bending action, which would tend to dilate

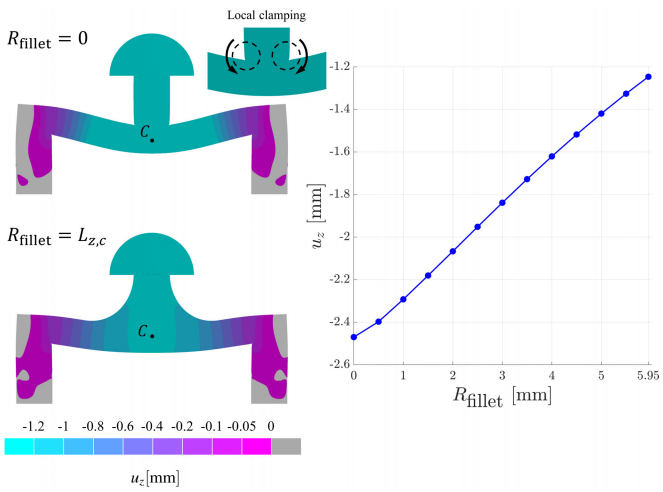

Fig. 3. Parametric analysis of the fillet radius—R_{fillet}. Vertical displacement field (left, with the deformation factor of the deformed configuration equal to unity) and vertical displacement of the central point of the centerline (right).

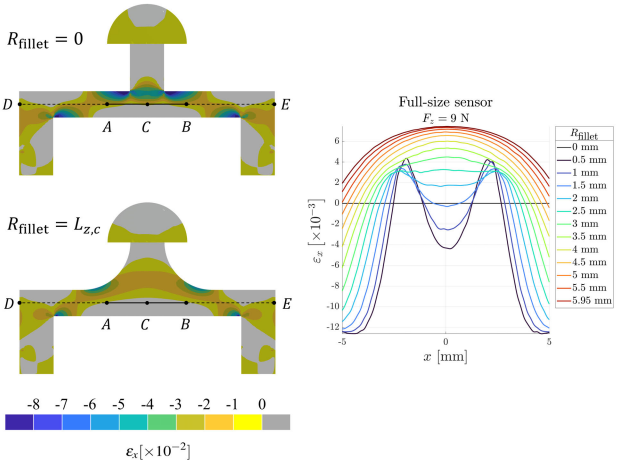

Fig. 4. Parametric analysis of the fillet radius R_{fillet}. Axial strain $\langle \varepsilon_X \rangle$ field for the $R_{\text{fillet}} = 0$ (left, top) and the $R_{\text{fillet}} = L_{z,c}$ (left, bottom) cases and axial strain ex along the FBG segment AB (right).

the centerline ($\varepsilon_x > 0$), and a clamping action of the central column, which causes local contraction in a neighborhood of the fillet region ($\varepsilon_x < 0$). This is evident in Fig. 4 (right), where it is shown that in the vicinity of sharp fillet radii (e.g., $R_{\text{fillet}} = 0$), the axial strain $\varepsilon_x(x)$ along the FBG segment varies experiencing rapid variations from positive to negative values, and this is visually seen again in Fig. 4 (left, top), where the FBG segment AB lays almost entirely within the $\varepsilon_x < 0$ region. Conversely, for higher fillet values (e.g., $R_{\text{fillet}} = L_{z,c}$), no such variations occur and the FBG segment remains within the $\varepsilon_x > 0$ region (see Fig. 4, left, bottom). The variation of $\langle \varepsilon_x \rangle$ with respect to R_{fillet}, shown in Fig. 5 (left), highlights that there is a threshold value R^*_{fillet} (in our studied geometry, $R^*_{\text{fillet}} \simeq 1.8$ mm) below which the FBG segment is compressed on average, suggesting a poor performance of the sensor. Above R^*_{fillet}, $\langle \varepsilon_x \rangle$ increases to progressively higher positive values, although it should be noted that the slope of the curve in Fig. 5 (left) decreases with R_{fillet}, suggesting that from the structural point of view, it is unnecessary to have fillets excessively larger than the threshold value R^*_{fillet}, since they will yield only marginally higher $\langle \varepsilon_x \rangle$. As a result, the choice of R_{fillet} must consider

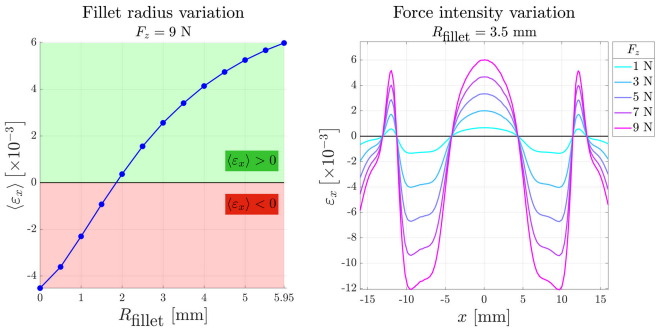

Fig. 5. Parametric analyses compared. Influence of the fillet radius on the average axial strain—$\langle \varepsilon_X \rangle$ at constant force value (left) and influence of the F_Z value on the axial strain—ε_X at constant fillet radius (right).

not only the threshold R^*_{fillet} associated with the structural performance of the sensor, which would require fillets well above R^*_{fillet}, but fabrication and technological aspects as well (for instance, the printability of fillets very close to or far from the threshold). In this work, we have considered a fillet of $R_{\text{fillet}} = 3.5$ mm $\simeq 2R^*_{\text{fillet}}$, a reasonable tradeoff between structural performance and technical feasibility.

Lastly, it is interesting to notice that for a fixed value of R_{fillet}, the variation of the intensity of the applied F_z alters the structural response along the centerline only in terms of the intensity of the axial strain $\varepsilon_x(x)$, as Fig. 5 (right) illustrates. The null points of the curves, however, occur at the same locations.

C. Fabrication

An FBG sensor (grating length of 10 mm, λ_B of 1549 nm, and reflectivity >90%, AtGrating) was integrated into the external structure optimized by the FEM analysis described in Section II-B. All the components of the tactile sensor were created using a 3-D printer (Sovol SV04) based on FDM.

The contact head was printed in PLA, while the rest of the structure in which the FBG is embedded including the central column was printed in TPU 95A. Making the contact head more rigid allowed the transmission of the entire F_z exerted on it to the body structure and, consequently, to the enclosed FBG.

The manufacturing process of the tactile sensor consists of three main steps.

1) Three-Dimensional Model Design: The 3-D model of the sensor is designed using a CAD software (Onshape), as shown in Fig. 6.

2) Setting of Printing Parameters: The CAD is sent to the slicing software CURA. This step consists of the generation of a g.code file with the following printing settings: the infill density of 100%, triangle pattern, and printing speed of 30 mm/s.

3) Three-Dimensional Printing: The printing starts. The molted filament is extruded by the nozzle and deposited layer-by-layer. The dual mode of the 3-D printer is used to print both the bridge-like structure and the contact head. At the 40th layer of the U-shaped structure, the channel to embed the fiber is created, and the printer is stopped. After that, the fiber is pretensioned into the channel using a couple of magnets (see Fig. 6), the printer is resumed, and the fiber is integrated into the structure. At the end of the 3-D printing, the U-shaped structure and the contact head are removed from the plate. The 3-D-printed contact head has a cavity precisely

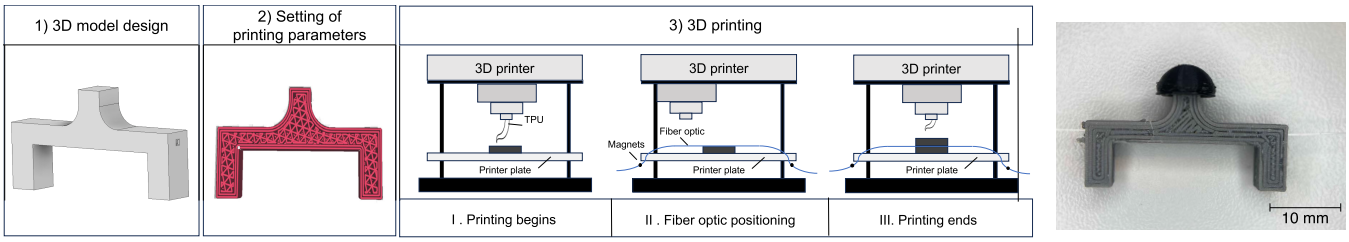

Fig. 6. Main fabrication steps of the U-shaped structure: from the 3-D model design to the 3-D printing, including the FBG integration and the final prototype with a reference scale.

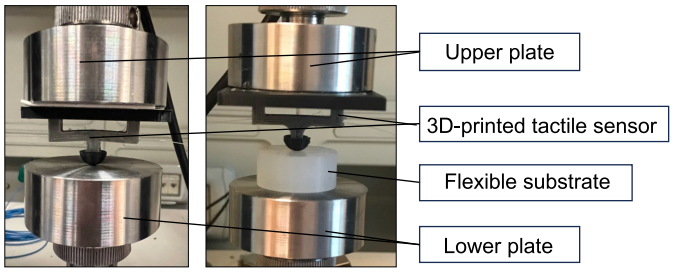

Fig. 7. Tactile sensor is pushed against the stainless steel material (left) and a silicone substrate (right).

designed to align with the central column of the U-shaped structure.

Fig. 6 shows the fabrication steps with a focus on the U-shaped structure that encapsulates the FBG sensor.

III. Experiments and Results

A. Experimental Setup and Protocol

Once the fabrication phase ended, the sensing core with the optimized design was tested to assess its response under loading conditions. A range of F from ~0 N to 9 N was applied by performing a compression test. These F values were chosen to extensively cover the F range exerted on the sensor during superficial palpation of soft tissues like the breast [32]. Indeed, the proposed sensing element is intended to work in an array configuration. Hence, when pushed against the tissue, F at the tissue–probe interface will be equally distributed according to the number of sensors integrated into the tactile probe (e.g., three sensing elements in [32]). The experimental setup consists of a testing machine (Instron mod. 3365) used to apply loads and record the machine output (i.e., the exerted F and displacement). The sensor was positioned on the upper machine plate to mimic its working condition once integrated into the tactile probe and an optical interrogator (si255 Hyperion Platform, Luna Inc.) was used to record the output of the FBG. Both the compression machine and the interrogation unit recorded data at a sampling rate of 100 Hz. To investigate the response of the proposed sensor to materials with different stiffness, the compression test was performed by pushing the sensing unit against different substrates made of stainless steel (E = 190 GPa), Dragon skin 30 (E = 1.41 MPa), Dragon skin 10 (E = 550 kPa), and Ecoflex 30 (E = 70 kPa), as shown in Fig. 7. For each material, seven repetitions of the compression test were performed to assess the repeatability of the sensor response to F at quasi-static conditions by setting a compression velocity of 2 mm/min.

B. Data Analysis

The recorded data were analyzed in MATLAB environment as follows. First, data related to F and displacement of the compression machine and $\Delta\lambda_B$ values of the FBG were synchronized to investigate the sensor response to F for each material (Fig. 7). The mean $\Delta\lambda_B$ versus F trend was obtained by averaging the $\Delta\lambda_B$ versus F curves of the seven repetitions for each material, (see black line in Fig. 8).

Furthermore, the best fitting curve of the mean $\Delta\lambda_B$ versus F trend was computed to obtain the calibration curve (red line in Fig. 8), and the expanded uncertainty was estimated to investigate the repeatability in the sensor response considering a t-student distribution with a level of confidence of 95% and a number of degrees of freedom equal to six.

C. Results

The results showed that the proposed sensor experienced tension when pushed against different materials. It means that the FEM-guided design optimization makes the embedding structure able to transduce F applied on its contact head into a positive ε of the FBG enclosed in the central part. Fig. 8 shows the response of the FBG in terms of mean and expanded uncertainty when the 3-D-printed structure is pushed against the four materials from the more rigid (the stainless steel) to the more flexible (the Ecoflex 30). From trends in Fig. 8, apparently, inappreciable differences in the sensor output occurred with F for materials with different E values. Indeed, Fig. 8 shows that the sensor reached approximately the same $\Delta\lambda_B$ value at the end of each test (for F = 9 N).

On the contrary, when examining the sensor response in relation to the displacement recorded by the compression machine ($\Delta\lambda_B$ versus displacement) for F value ranging from ~0 to 9 N [see Fig. 9(a)], it becomes evident that the compression machine recorded higher displacement when the sensor is pushed against more rigid materials: under the same applied F on the contact head, the higher the E value, the lower the attained displacement. This behavior can be motivated considering that the displacement recorded by the compression machine is the sum of the displacement of the sensor and the displacement experienced by the silicone material. When pressed against a stiffer material, such as steel, the 3-D-printed structure deforms almost immediately, while the steel plate remains practically undeformed. In this case, the recorded displacement coincides with the deformation of the 3-D-printed sensor only. In contrast, when the sensor is pressed against a softer material, such as silicone, the flexible substrate absorbs energy to deform. This energy needs to be distributed through the material before it can offer significant resistance to the sensor. Once the thickness of the softer material is significantly reduced, the 3-D-printed sensor starts to deform. In the first part, the displacement recorded by the machine is mainly related to the squashing of the flexible material. In this part, the output of the sensor is ~0 nm. This behaviour can be

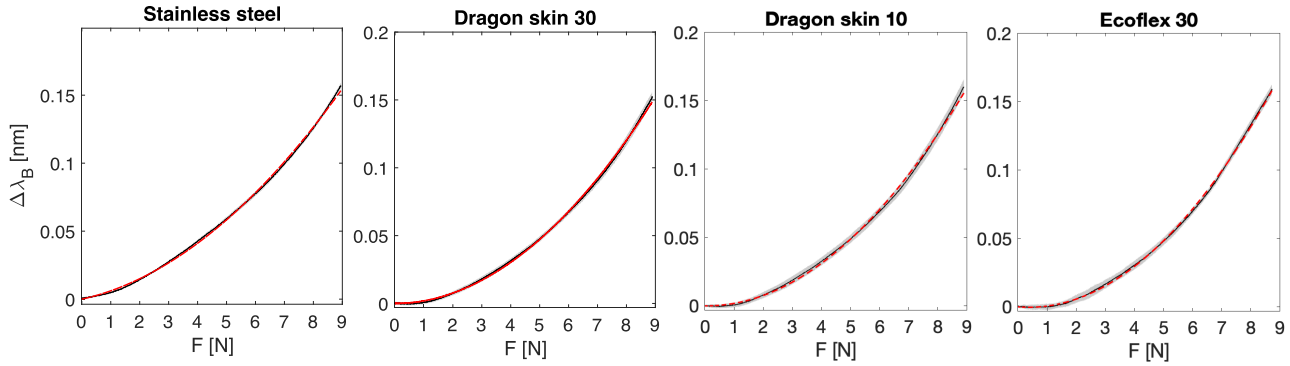

Fig. 8. Three-dimensional-printed tactile sensor response to F when pushed against the stainless steel, Dragon skin 30, Dragon skin 10, and Ecoflex 30 materials: the experimental data (i.e., mean $\Delta\lambda_B$ versus F trends) are plotted in black lines, the calibration curves in red lines, and the expanded uncertainty in shadow gray areas.

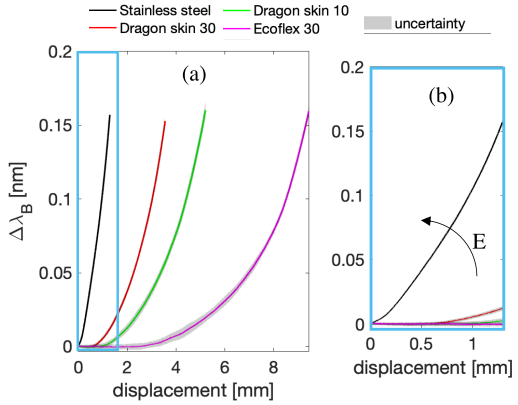

Fig. 9. (a) Three-dimensional-printed tactile sensor response to displacement when pushed against the stainless steel (black line), Dragon skin 30 (red line), Dragon skin 10 (green line), and Ecoflex 30 (magenta line) materials in terms of the mean $\Delta\lambda_B$ versus displacement trend and expanded uncertainly in the shadow gray area. (b) Zoom on the 3-D-printed tactile sensor response to displacement to emphasize changes in the mean $\Delta\lambda_B$ versus displacement trends with E.

seen in Fig. 9 where the sensor responded immediately when pushed against the stainless steel (the more rigid material), while its response is ∼0 nm at the beginning of the tests on flexible materials. This phenomenon is more emphasized in Fig. 9(b), by zooming the $\Delta\lambda_B$ versus displacement trends in the smallest displacement range (i.e., from 0 to 1.3 mm). As expected, the best response to displacement was experienced by the sensor when pushed against the hardest material (i.e., a sensitivity to displacement of 0.12 nm/mm for the stainless steel material that reduces to 0.01 nm/mm for Dragon skin 30, to 0.002 nm/mm for Dragon skin 10, and to ∼0 nm/mm for Ecoflex 30). These results suggest the capability of the proposed system to discriminate tissues with different rigidities, showing promising performance for tactile sensing in tumor identification applications.

IV. Discussion

This study proposed an optimization of the structural design of the sensing unit of the tactile probe recently proposed in [32] for tumor identification. A FEM-guided analysis was carefully carried out to propose a key change in the shape of the 3-D-printed structure in terms of R_{fillet} to lead the enclosed FBG sensor to work in tension. This response is preferable when working with FBG technology, preserving their integrity during operation.

In the literature, only a few studies investigated the use of a similar technology for tissue palpation based on tactile sensing. Most are developed for MIS and robotic MIS applications and integrate FBG sensors by directly pasting the optical fiber on the internal and external surfaces of the shaft or directly on the end of the instrument. This sensor placement requires that the surgical instruments must be cleaned and disinfected before and after each use [19], [28], [29], [30], [31]. Moreover, the glue layer may cause the nonuniform F transmission to the enclosed FBG. A similar system was proposed in [19]. The tactile sensor is composed of five identical tactile cells. Each cell is composed of a spiral elastomer, a suspended FBG sensor glued to the two sides of the elastomer, and a contact head. The designed sensor was first calibrated over the F range from ∼0 N to 1 N. Then, palpation experiments were performed on silicone with three rigid parallelepiped-shaped blocks enclosed in the material to simulate tumors. These tests consisted of slow indentation operations within the range of 0 mm–1.5 mm on four positions. Three of these indentation positions correspond to the block locations and one without blocks. Results showed an increase in the sensor output according to the presence of the blocks and their indentation depth. As in [19], the sensor proposed in the present study experienced a positive ε response when pressed against materials with different stiffnesses. This behavior was guided by the FEM analysis. FEM results showed that the local clamping effects occurring in the previous design could be overcome by using an $R_{\text{fillet}} \geq 1.8$ mm. In this study, we used an R_{fillet} of 3.5 mm, which is approximately two times higher than the threshold. In this way, the sensing length of the enclosed FBG will not be subjected to the local effects imposed by 90° geometry angles, and a tradeoff between structural performance and technical feasibility can be guaranteed. Moreover, our solution does not require the use of glue to fix the optical fiber to the structure. We performed the FBG integration guaranteeing a pretensioning state using a couple of magnets in steps II and III of the fabrication stage 3-D printing in Fig. 6. In this way, no additional materials are interfaced between the FBG and the printed materials. Moreover, the integration of the FBG into a 3-D-printed structure makes the system easy to reuse and sterilizable. Finally, its working ranges in terms of both F and displacement values are larger

than those in [19], extending the use of the proposed sensor on a wider range of tissues with different mechanical properties from softer (e.g., breasts and prostates) to stiffer (e.g., cancers and bones).

V. Conclusion

This work proposed a design optimization of a 3-D-printed tactile sensor based on FBG technology for tumor identification via tactile sensing. The results of the FEM analysis highlighted that an R_{fillet} of 3.5 mm is a good compromise to eliminate the local clamping effect that caused compression on the FBG in [32] with a reduced stiffness for the proposed system. Otherwise, higher R_{fillet} values are expected to improve the system rigidity. This novel design suggests that the FEM analysis is a valuable tool in the sensor design process, providing insights into structural aspects to improve the system performance. Tests on materials with different rigidities showed that the FBG enclosed in the proposed structure works in tension when pressed against these substrates with promising capacities of discriminating materials with different mechanical properties. Future tests will be devoted to reduce the dimensions of the proposed sensing solution to create an array of tactile sensors with higher spatial resolution. The array will be able to perform differential measurements for identifying tumors in human tissues. A FEM will guide the design miniaturization to guarantee high performance of the single unit and reduce the crosstalk effects. Tests on a silicone phantom embedding plastic elements to mimic a biological tissue with tumors will be carried out for assessing the palpation capacity of the proposed system. Then, tests on healthy volunteers and patients diagnosed with a tumor will be performed to evaluate the system performance in real clinical settings. In the field of medical diagnostics, the use of a highly performant tactile sensor array for tumor identification through superficial tissue palpation will be fundamental for enhancing early detection capabilities, improving accuracy, and ultimately advancing the efficacy of prevention measures.

References

[1] J. Konstantinova, M. Li, G. Mehra, P. Dasgupta, K. Althoefer, and T. Nanayakkara, "Behavioral characteristics of manual palpation to localize hard nodules in soft tissues," *IEEE Trans. Biomed. Eng.*, vol. 61, no. 6, pp. 1651–1659, Jun. 2014, doi: 10.1109/TBME.2013.2296877.

[2] L. Jacobs, "Positive margins: The challenge continues for breast surgeons," *Ann. Surg. Oncol.*, vol. 15, no. 5, pp. 1271–1272, May 2008, doi: 10.1245/S10434-007-9766-0.

[3] A. El Saddik, "The potential of haptics technologies," *IEEE Instrum. Meas. Mag.*, vol. 10, no. 1, pp. 10–17, Feb. 2007, doi: 10.1109/MIM.2007.339540.

[4] P. Puangmali, K. Althoefer, L. D. Seneviratne, D. Murphy, and P. Dasgupta, "State-of-the-art in force and tactile sensing for minimally invasive surgery," *IEEE Sensors J.*, vol. 8, no. 4, pp. 371–380, Apr. 2008, doi: 10.1109/JSEN.2008.917481.

[5] W. Wang, J. Wang, Y. Luo, X. Wang, and H. Song, "A survey on force sensing techniques in robot-assisted minimally invasive surgery," *IEEE Trans. Haptics*, vol. 16, no. 4, pp. 702–718, Oct. 2023, doi: 10.1109/toh.2023.3329172.

[6] C. Chi, X. Sun, N. Xue, T. Li, and C. Liu, "Recent progress in technologies for tactile sensors," *Sensors*, vol. 18, no. 4, p. 948, Mar. 2018, doi: 10.3390/s18040948.

[7] K. Navindaran, J. S. Kang, and K. Moon, "Techniques for characterizing mechanical properties of soft tissues," *J. Mech. Behav. Biomed. Mater.*, vol. 138, Feb. 2023, Art. no. 105575, doi: 10.1016/j.jmbbm.2022.105575.

[8] K. Hoyt et al., "Tissue elasticity properties as biomarkers for prostate cancer," *Cancer Biomarkers*, vol. 4, nos. 4–5, pp. 213–225, Nov. 2008, doi: 10.3233/cbm-2008-44-505.

[9] C.-H. Won, J.-H. Lee, and F. Saleheen, "Tactile sensing systems for tumor characterization: A review," *IEEE Sensors J.*, vol. 21, no. 11, pp. 12578–12588, Jun. 2021, doi: 10.1109/JSEN.2021.3078369.

[10] W. Othman et al., "Tactile sensing for minimally invasive surgery: Conventional methods and potential emerging tactile technologies," *Frontiers Robot. AI*, vol. 8, Jan. 2022, Art. no. 705662, doi: 10.3389/frobt.2021.705662.

[11] J. Carlsen et al., "Ultrasound elastography in breast cancer diagnosis," *Ultraschall der Medizin-Eur. J. Ultrasound*, vol. 36, no. 6, pp. 550–565, Aug. 2015, doi: 10.1055/s-0035-1553293.

[12] B. S. Garra et al., "Elastography of breast lesions: Initial clinical results," *Radiology*, vol. 202, no. 1, pp. 79–86, Jan. 1997, doi: 10.1148/radiology.202.1.8988195.

[13] R. Sinkus, J. Lorenzen, D. Schrader, M. Lorenzen, M. Dargatz, and D. Holz, "High-resolution tensor MR elastography for breast tumour detection," *Phys. Med. Biol.*, vol. 45, no. 6, pp. 1649–1664, Jun. 2000, doi: 10.1088/0031-9155/45/6/317.

[14] J. Kemper, R. Sinkus, J. Lorenzen, C. Nolte-Ernsting, A. Stork, and G. Adam, "MR elastography of the prostate: Initial in-vivo application," *RöFo-Fortschritte auf dem Gebiet der Röntgenstrahlen und der bildgebenden Verfahren*, vol. 176, no. 8, pp. 1094–1099, Aug. 2004, doi: 10.1055/s-2004-813279.

[15] S. E. Cross, Y.-S. Jin, J. Rao, and J. K. Gimzewski, "Nanomechanical analysis of cells from cancer patients," *Nature Nanotechnol.*, vol. 2, no. 12, pp. 780–783, Dec. 2007, doi: 10.1038/nnano.2007.388.

[16] A. Calzado-Martín, M. Encinar, J. Tamayo, M. Calleja, and A. S. Paulo, "Effect of actin organization on the stiffness of living breast cancer cells revealed by peak-force modulation atomic force microscopy," *ACS Nano*, vol. 10, no. 3, pp. 3365–3374, Mar. 2016.

[17] D. Lo Presti et al., "Fiber Bragg gratings for medical applications and future challenges: A review," *IEEE Access*, vol. 8, pp. 156863–156888, 2020, doi: 10.1109/ACCESS.2020.3019138.

[18] A. A. Abushagur, N. Arsad, M. I. Reaz, and A. A. Bakar, "Advances in bio-tactile sensors for minimally invasive surgery using the fibre Bragg grating force sensor technique: A survey," *Sensors*, vol. 14, no. 4, pp. 6633–6665, 2014, doi: 10.3390/s140406633.

[19] T. Li, C. Shi, and H. Ren, "A high-sensitivity tactile sensor array based on fiber Bragg grating sensing for tissue palpation in minimally invasive surgery," *IEEE/ASME Trans. Mechatronics*, vol. 23, no. 5, pp. 2306–2315, Oct. 2018, doi: 10.1109/TMECH.2018.2856897.

[20] L. Massari, C. M. Oddo, E. Sinibaldi, R. Detry, J. Bowkett, and K. C. Carpenter, "Tactile sensing and control of robotic manipulator integrating fiber Bragg grating strain-sensor," *Frontiers Neurorobotics*, vol. 13, Apr. 2019, Art. no. 434583, doi: 10.3389/fnbot.2019.00008.

[21] J.-S. Heo, J.-H. Chung, and J.-J. Lee, "Tactile sensor arrays using fiber Bragg grating sensors," *Sens. Actuators A, Phys.*, vol. 126, no. 2, pp. 312–327, Feb. 2006.

[22] D. Lo Presti et al., "A wearable flower-shaped sensor based on fiber Bragg grating technology for in-vivo plant growth monitoring," *IEEE Sensors J.*, vol. 23, no. 8, pp. 8416–8425, Apr. 2023, doi: 10.1109/JSEN.2023.3253782.

[23] Y. Kuang, Y. Guo, L. Xiong, and W. Liu, "Packaging and temperature compensation of fiber Bragg grating for strain sensing: A survey," *Photonic Sensors*, vol. 8, no. 4, pp. 320–331, Dec. 01, 2018, doi: 10.1007/s13320-018-0504-y.

[24] D. Lo Presti et al., "Wearable system based on flexible FBG for respiratory and cardiac monitoring," *IEEE Sensors J.*, vol. 19, no. 17, pp. 7391–7398, Sep. 2019, doi: 10.1109/JSEN.2019.2916320.

[25] W. Yan, S. Ma, H. Wang, and X. Zhang, "Fiber Bragg grating online packaging technology based on 3D printing," *Opt. Laser Technol.*, vol. 131, Nov. 2020, Art. no. 106443, doi: 10.1016/j.optlastec.2020.106443.

[26] D. L. Presti et al., "The effect of infill pattern and density on the response of 3-D-printed sensors based on FBG technology," *IEEE Sensors J.*, vol. 22, no. 20, pp. 19357–19365, Oct. 2022, doi: 10.1109/JSEN.2022.3202101.

[27] T. Erdogan, "Fiber grating spectra," *J. Lightw. Technol.*, vol. 15, no. 8, pp. 1277–1294, Aug. 1997, doi: 10.1109/50.618322.

[28] Z. Wu, A. Gao, N. Liu, Z. Jin, and G.-Z. Yang, "FBG-based triaxial force sensor integrated with an eccentrically configured imaging probe for endoluminal optical biopsy," in *Proc. IEEE Int. Conf. Robot. Autom. (ICRA)*, May 2020, pp. 1625–1631, doi: 10.1109/ICRA40945.2020.9197128.

[29] A. Gao, Y. Zhou, L. Cao, Z. Wang, and H. Liu, "Fiber Bragg grating-based triaxial force sensor with parallel flexure hinges," *IEEE Trans. Ind. Electron.*, vol. 65, no. 10, pp. 8215–8223, Oct. 2018, doi: 10.1109/TIE.2018.2798569.
[30] Z. Zhang, C. Zhang, and S. Zuo, "A novel bioinspired whisker sensor for gastrointestinal endoscopy," *IEEE/ASME Trans. Mechatronics*, vol. 29, no. 1, pp. 636–646, Feb. 2024, doi: 10.1109/TMECH.2023.3289955.
[31] R. Ben Hassen, A. Lemmers, and A. Delchambre, "Tri-axial force sensor in a soft catheter using fiber Bragg gratings for endoscopic submucosal dissection," *IEEE Sensors J.*, vol. 23, no. 20, pp. 24626–24636, Oct. 2023, doi: 10.1109/JSEN.2023.3313172.
[32] D. Lo Presti et al., "A 3-D-printed tactile probe based on fiber Bragg grating sensors for noninvasive breast cancer identification," *IEEE Sensors J.*, vol. 23, no. 20, pp. 24489–24499, Oct. 2023, doi: 10.1109/JSEN.2023.3306970.
[33] D. Feng, X. Luo, Y. Liu, C. Ma, and X. Qiao, "Performance improvement of FBG sensors based on the pre-stressed package technique," *Opt. Fiber Technol.*, vol. 65, Sep. 2021, Art. no. 102623, doi: 10.1016/j.yofte.2021.102623.
[34] J. Ang, H. C. H. Li, I. Herszberg, M. K. Bannister, and A. P. Mouritz, "Tensile fatigue properties of fibre Bragg grating optical fibre sensors," *Int. J. Fatigue*, vol. 32, no. 4, pp. 762–768, Apr. 2010, doi: 10.1016/j.ijfatigue.2009.11.002.

D. Lo Presti (Member, IEEE) received the Ph.D. degree from Università Campus Bio-Medico di Roma, Rome, Italy, in 2021.

She is currently an Assistant Professor with the Unit of Measurements and Biomedical Instrumentation of Università Campus Bio-Medico di Roma. Her main research activities focus on the design, fabrication, and feasibility assessment of smart systems and wearables based on fiber optics for biomedical applications.

L. Zoboli received the Ph.D. degree from Università Campus Bio-Medico di Roma, Rome, Italy, in 2022.

He is a Postdoctoral Researcher of Solid and Structural Mechanics with Università Campus Bio-Medico di Roma. Currently, he is investigating nonlinear coupled phenomena during the curing phase of polymers. His research activity focuses on polymer modeling, multiscale mechanics, coupled physics, nuclear fusion, and finite element analysis.

Dr. Zoboli is a member of AIMETA and Indam-GNFM.

A. Addabbo is currently pursuing the master's degree in biomedical engineering with Università Campus Bio-Medico di Roma, Rome, Italy.

His expertise is in the field of design, fabrication, and metrological assessment of measuring systems for biomedical applications.

D. Bianchi received the Ph.D. degree from Università Campus Bio-Medico di Roma, Rome, Italy, in 2018.

He is an Assistant Professor with Università Campus Bio-Medico di Roma. His main research interests include the mathematical modeling of tissue biomechanics, computational mechanics, and topological optimization for additive manufacturing.

A. Dimo (Student Member, IEEE) received the M.Sc. degree from Università Campus Bio-Medico di Roma, Rome, Italy, in 2022.

He is a Scientific Research Collaborator with the Unit of Measurements and Biomedical Instrumentation, Università Campus Bio-Medico di Roma. His research interests include the design and development of FBG-based systems for biomedical applications.

C. Massaroni (Senior Member, IEEE) received the Ph.D. degree from Università Campus Bio-Medico di Roma, Rome, Italy, in 2017.

He is an Assistant Professor with the Unit of Measurements and Biomedical Instrumentation, Università Campus Bio-Medico di Roma. His research interests include the design, development, and test of wearable devices and unobtrusive measuring systems for medical applications.

Dr. Massaroni has been the Chair of the "Wearable Sensors" TC of the Italy Chapter of the IEEE Sensors Council since 2020.

V. Altomare is a Full Professor of General Surgery with Campus Bio-Medico University of Rome, Rome, Italy. He is the Director of the Breast Surgical Unit of Campus Bio-Medico Hospital Foundation. His main research interests include breast cancer management and oncoplastic surgical treatment.

A. Grasso received the Ph.D. degree from Campus Bio-Medico University Hospital Foundation, Rome, Italy, in 2019.

She is a Consultant Breast Surgeon with Campus Bio-Medico University Hospital Foundation. Her main field of interest is prevention, diagnosis, and treatment of breast diseases. Her research interests include oncoplastic surgery and targeted surgical therapies.

A. Gizzi (Senior Member, IEEE) received the Ph.D. degree from Università Campus Bio-Medico di Roma, Rome, Italy, in 2012.

He is an Associate Professor of Solid and Structural Mechanics with Università Campus Bio-Medico di Roma. His main research interests include theoretical and computational biomechanics and mechanobiology.

Dr. Gizzi has been a member of the Executive Board of the European Society of Biomechanics–Italy Chapter and IEEE-EMBS member since 2023.

E. Schena (Senior Member, IEEE) received the Ph.D. degree from Università Campus Bio-Medico di Roma, Rome, Italy, in 2007.

He is a Full Professor of Measurements with Università Campus Bio-Medico di Roma. His research interests include the design and assessment of wearables and measuring systems for human health monitoring.

Dr. Schena was the Chair of the Italy Chapter of the IEEE Sensors Council in 2018.

Open Access funding provided by 'Università "Campus Bio-Medico" di Roma' within the CRUI CARE Agreement